Film–Forming Kinetics in Organic Solar Cells

Subjects: Nanoscience & Nanotechnology

Contributor: Jiangang Liu

Solution–processed organic solar cells (OSC) have been explored widely due to their low cost and convenience, and impressive power conversion efficiencies (PCEs) which have surpassed 18%. In particular, the optimization of film morphology, including the phase separation structure and crystallinity degree of donor and acceptor domains, is crucially important to the improvement in PCE. Considering that the film morphology optimization of many blends can be achieved by regulating the film–forming process, it is necessary to take note of the employment of solvents and additives used during film processing, as well as the film–forming conditions.

organic solar cells | solution process | morphology | film–forming kinetics

1. Introduction

Organic solar cells (OSCs) have been recognized as one of the most promising green devices to convert solar energy to electricity, which possesses the advantages of light weight, flexibility, processable printing and large–area production [1][2][3][4]. OSCs consist of an anode, cathode and active layer. By 2021, thanks to the favorable development of donor and acceptor materials, optimization of active layer morphology and maturity of processing technology, the OSCs have realized outstanding power conversion efficiency (PCE), over 18% for binary devices [5][6][7][8][9][10][11][12]. These devices based on a ternary active layer can achieve the same or better performance [13][14][15][16][17][18][19].

The performance of OSC devices is closely related to the morphology of the active layer, because it crucially affects the photophysical conversion process. The photophysical conversion process usually includes photon absorption (exciton generation), exciton diffusion, exciton separation, carrier transport and collection [20]. After the active layer absorbs a photon, the electron in the donor's highest occupied molecular orbital (HOMO) is excited and jumps to the donor's lowest unoccupied molecular orbital (LUMO) to form an electron–hole pair bounded by coulomb forces. Because of the strong binding energy (0.35~0.5 eV), the exciton cannot be separated through thermal vibration [21][22]. Therefore, the exciton separation can only rely on the electric field gravity provided by the built–in electric field at the donor/acceptor (D/A) interfaces. However, if the domain size is too large, some excitons cannot reach the D/A interfaces due to their short lifetime [23][24]. Only the excitons near the D/A interface (5~10 nm) can reach the interfaces and have the chance to dissociate into electrons and holes driven by the built–in electric field. Therefore, the suitable domain size is usually 10~20 nm in OSCs [25][26]. According to previous research, the molecular orientation of the donor and acceptor at the interface directly determines the driving forces of the built–in electric field [27]. When the orientation of the donor and acceptor is consistent, the coupling force between the donor and acceptor is large, leading to a strong built–in electric field, which is beneficial for exciton

dissociation [28][29][30]. Furthermore, generated free electrons and holes need to transport to the corresponding anode and cathode through the pure acceptor and donor phases, respectively. Hence, the bi–continuous separated donor and acceptor phases, i.e., an interpenetrating network structure (**Figure 1**), is highly desirable for carrier transmission [31][32][33][34][35]. In addition, high carrier mobility ensures the efficiency of charge collection, hence a high crystallinity degree of the donor and acceptor is required because it reduces the energy barrier of charge transport and helps to obtain high carrier mobility [36][37][38][39][40][41]. Additionally, the donor and acceptor should be enriched at the anode and cathode, respectively, which can effectively reduce the bimolecular recombination, thereby improving the charge collection [42]. According to the relationship between the morphology of the active layer and the photoelectric process of devices, it is obvious that the active layer should possess a highly crystalline interpenetrating network with a proper domain size and face–on molecular orientation.

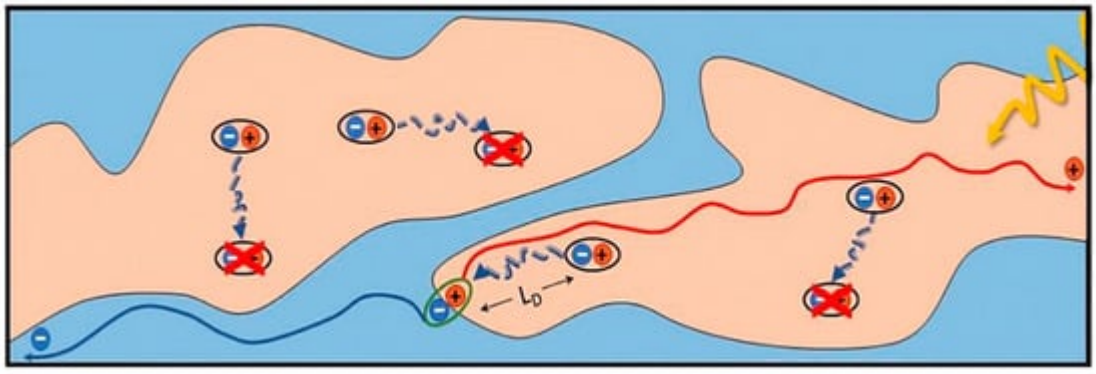

Figure 1. Schematic illustration of exciton dissociation and carrier transport in large phase domains. Reproduced from [43]. Reprinted with permission from ref. [43]. Copyright 2018 MDPI.

Therefore, on the basis of molecular tailoring [44][45], researchers have invented a variety of methods for optimizing the morphology of the active layer. One of most widely used effective methods is thermal annealing (TA), which can enhance the molecular stack and degree of crystallinity of the donor and acceptor [46][47][48][49][50]. For example, in P3HT:SF–HR–blend thin films, the diffraction intensity becomes much clearer, which means the degree of crystallinity of both the donor and acceptor increases dramatically after TA at 120 °C [51]. Similar to TA, solvent vapor annealing (SVA) is also an effective method to optimize the film morphology [52][53][54][55][56]. Hou et al. used a dichloromethane SVA–treated DRTB–T:IC–C6IDT–IC–based blend film for 60 s, and the ordered aggregation of donor and acceptor was promoted, which facilitated the formation of an interpenetrating network structure. This optimized phase separation structure is conducive to the exciton dissociation and carrier transport, boosting the PCE of the device from 5.03% to 9.08% [57]. However, it is a challenge to combine the two methods for practical large area manufacture, for TA is difficult to employ to treat flexible substrates of low glass transition temperature, and SVA is not compatible with the roll–to–roll process [58][59]. A number of research teams have recently made advances without using either method [60][61][62][63].

Furthermore, the morphology of the BHJ active layer closely depends on the film–forming process of solution processing [64][65][66][67][68]. During the evaporation of the solvent, the solution layer gradually evolves from the liquid state to solid state on the substrate, and the formed film is frozen in a thermodynamic metastable state. The

film–forming process decides the film quenching depth of the frozen state. For example, through extending the film–forming time, the donor and acceptor molecules have sufficient time to diffuse and rearrange, leading to enhanced crystallinity of the film and increased domain sizes. If the donor and acceptor are precipitated simultaneously in a short time during the film–forming process, the degree of crystallinity of both the donor and acceptor is low due to the insufficient self–aggregating time. Therefore, controlling the kinetics of film–forming process can also regulate the morphology of the active layer.

This entry focuses on the influence of the film–forming kinetics process on the morphology of the active layer in OSCs, and the underlying mechanisms are revealed. Furthermore, methods used to regulate the film–forming kinetics process are summarized and representative examples are given and discussed to understand the key parameters of tuning the film–forming process. Finally, a future control and development of film–forming kinetics is briefly outlined, which may give some guidance to achieve a high PCE of OSCs. Here, we summarize in **Table 1** the critical works on film–forming kinetics in OSCs, and the cartoon illustration is shown in **Figure 2**.

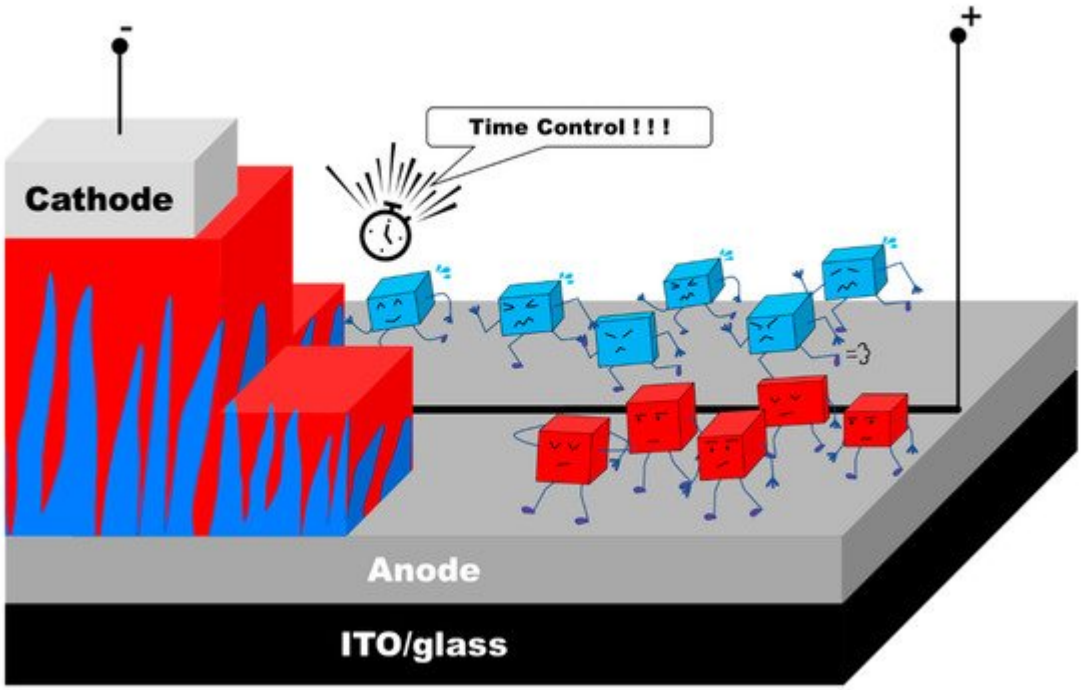

Figure 2. Cartoon illustration of film–forming dynamics.

Table 1. Summary of the performance of the OSC's active layer previously reported (some full names corresponding to the abbreviations are listed below).

Active Layer	Conditions	V_{OC} [V]	J_{SC} [mA cm^{-2}]	FF [%]	PCE$_{max}$ [%]	Ref.
P3HT:PCBM	Solvent CB	0.64	1.63	52.3	0.58	[69]
	Additive ODT 0.5%	0.55	8.23	68.8	3.13	

Active Layer	Conditions	V_{OC} [V]	J_{SC} [mA cm^{-2}]	FF [%]	PCE$_{max}$ [%]	Ref.
PTzBI–Si:N2200	Additive CN 4%	0.55	7.87	68.2	3.01	[70]
	Solvent CB	0.87	4.58	51.14	2.04	
	Solvent MTHF	0.88	17.62	75.78	11.76	
PBDB–T:INPIC–4F	Cast under strong SV	0.84	12.8	60.5	6.5	[71]
	Cast on 100 °C HS	0.82	21.8	73.2	13.1	
	Solvent CN	0.79	1.24	55	0.6	
PTB7–th:P(NDI2OD–T2)	Solvent *o*–DCB	0.77	6.82	51	2.86	[72]
	Solvent CB	0.78	8.86	50	3.63	
Ph–DTDP$_o$–OT:PBDB–T	Additive 1–CN 0.2%	0.87	15.00	58.60	7.65	[73]
Ph–DTDP$_o$–OTE:PBDB–T	Additive 1–CN 0.5%	0.88	18.28	68.57	10.98	
Ph–DTDP$_o$–TE:PBDB–T	Additive 1–CN 0.7%	0.82	20.83	71.14	12.21	
PDFQx3T:P(NDI2OD–T2)	Solvent CF	0.80	10.58	60	5.11	[74]
	Solvent CB	0.79	9.12	61	4.43	
	Solvent DCB	0.80	8.44	60	4.04	
	Solvent XY	0.79	7.91	61	3.83	
	Solvent CF	0.907	16.8	62.57	9.72	
FTAZ:ITIC–Th	Additive ODT:DIO 0.375%:0.125%	0.922	17.78	66.64	11.15	[75]
P3HT:O–IDTBR	Solvent CB	0.77	8.81	64	4.45	[42]
	Additive TCB 2%	0.76	13.49	70	7.18	
	Solvent CB	0.66	11.74	43	3.35	
PCPDTBT/C71–PCBM	Additive HS–C_8H_{16}–SH 2.5%	0.64	14.48	49	4.50	[76]
	Additive Br–C_8H_{16}–Br 2.5%	0.64	15.26	48	4.66	
	Additive I–C_8H_{16}–I 2.5%	0.61	15.73	53	5.12	
P3HT/PCBM	CB/tetralin 1:0.05	–	5.76	60	1.96	[77]

2. Summary and Perspectives

The photovoltaic performance of OSCs is closely related to the BHJ morphology of the active layer, because the crystallinity, molecular orientation, domain size and phase separation structure have a profound influence on the exciton dissociation, charge transport and collection. We know that the morphology of BHJ is a kinetically frozen structure. Hence, regulating the duration of the film–forming process, including solvent engineering and adjusting the substrate temperature, is an effective way to optimize the morphology of the active layer. The film–forming process contains solvent evaporation and solutes solidification, thus regulating the b.p. of solvents and spinning rate, and so is effective at optimizing the morphology. Specifically, prolonging the film–forming process could extend the duration of molecular diffusion, which is of benefit for the crystallization and phase separation; thus, high crystallinity and a large domain size with high phase purity were achieved. Moreover, the shortening of the film–forming process could promote the molecules to stay in a metastable state, in which the molecules tend to adopt face–on orientation. Furthermore, the selective solubility and high b.p. of the additive could also regulate the sequence of solidification between the donor and acceptor, promoting the formation of interpenetrating networks with optimized lateral phase separation. Overall, the examples demonstrated herein offer a rational guide to understanding the foundation of film–forming kinetics for optimizing the BHJ morphology of the active layer.

Presently, OSCs based on polymer/nonfullerene blends dominate the development of OSCs. The morphology optimization of the nonfullerene–based blend films empirically follows the various treatments originally developed in polymer/fullerene blends. Considering the different properties between nonfullerene and fullerene derivatives, such as solubility in solvent, miscibility between donor and acceptor and molecular diffusivity, morphology optimization should pay comprehensive attention to the molecular properties of the active layer, and rational morphology control treatments should be developed toward the combined goal of improved efficiency and increased stability. Additionally, solvent engineering is able to meet the requirements for the practical application of OSCs, such as the fabrication of large–area and flexible OSCs. Hence, thorough comprehension of film–forming kinetics in non–halogenated additives during large–area film–forming process should be taken into account to fabricate OSCs for their future application. The other important point is that existing research on film–forming kinetics does not elaborate on the relationship between kinetics and intermixed phases; although the study of intermixed phases is very complicated, kinetics may be used as a method to explore this field in the future.

References

1. Servaites, J.D.; Ratner, M.A.; Marks, T.J. Organic solar cells: A new look at traditional models. Energy Environ. Sci. 2011, 4, 4410–4422.
2. Service, R.F. Solar energy. Outlook brightens for plastic solar cells. Science 2011, 332, 293.
3. Dou, L.; You, J.; Hong, Z.; Xu, Z.; Li, G.; Street, R.A.; Yang, Y. 25th anniversary article: A decade of organic/polymeric photovoltaic research. Adv. Mater. 2013, 25, 6642–6671.

4. Krebs, F.C.; Espinosa, N.; Hosel, M.; Sondergaard, R.R.; Jorgensen, M. 25th anniversary article: Rise to power—OPV–based solar parks. Adv. Mater. 2014, 26, 29–38.
5. Liu, Q.; Jiang, Y.; Jin, K.; Qin, J.; Xu, J.; Li, W.; Xiong, J.; Liu, J.; Xiao, Z.; Sun, K.; et al. 18% Efficiency organic solar cells. Sci. Bull. 2020, 65, 272–275.
6. Song, J.; Zhu, L.; Li, C.; Xu, J.; Wu, H.; Zhang, X.; Zhang, Y.; Tang, Z.; Liu, F.; Sun, Y. High–efficiency organic solar cells with low voltage loss induced by solvent additive strategy. Matter 2021, 4, 2542–2552.
7. Meng, H.; Liao, C.; Deng, M.; Xu, X.; Yu, L.; Peng, Q. 18.77% Efficiency Organic Solar Cells Promoted by Aqueous Solution Processed Cobalt(II) Acetate Hole Transporting Layer. Angew. Chem. Int. Ed. 2021, 60, 22554–22561.
8. Liu, L.; Chen, S.; Qu, Y.; Gao, X.; Han, L.; Lin, Z.; Yang, L.; Wang, W.; Zheng, N.; Liang, Y.; et al. Nanographene–Osmapentalyne Complexes as a Cathode Interlayer in Organic Solar Cells Enhance Efficiency over 18. Adv. Mater. 2021, 33, e2101279.
9. Liu, G.; Xia, R.; Huang, Q.; Zhang, K.; Hu, Z.; Jia, T.; Liu, X.; Yip, H.L.; Huang, F. Tandem Organic Solar Cells with 18.7% Efficiency Enabled by Suppressing the Charge Recombination in Front Sub–Cell. Adv. Funct. Mater. 2021, 31, 2103283.
10. Li, C.; Zhou, J.; Song, J.; Xu, J.; Zhang, H.; Zhang, X.; Guo, J.; Zhu, L.; Wei, D.; Han, G.; et al. Non–fullerene acceptors with branched side chains and improved molecular packing to exceed 18% efficiency in organic solar cells. Nat. Energy 2021, 6, 605–613.
11. Jin, K.; Xiao, Z.; Ding, L. 18.69% PCE from organic solar cells. J. Semicond. 2021, 42, 060502.
12. Guo, C.; Li, D.; Wang, L.; Du, B.; Liu, Z.X.; Shen, Z.; Wang, P.; Zhang, X.; Cai, J.; Cheng, S.; et al. Cold–Aging and Solvent Vapor Mediated Aggregation Control toward 18% Efficiency Binary Organic Solar Cells. Adv. Energy Mater. 2021, 11, 2102000.
13. Zhang, T.; An, C.; Bi, P.; Lv, Q.; Qin, J.; Hong, L.; Cui, Y.; Zhang, S.; Hou, J. A Thiadiazole–Based Conjugated Polymer with Ultradeep HOMO Level and Strong Electroluminescence Enables 18.6% Efficiency in Organic Solar Cell. Adv. Energy Mater. 2021, 11, 2101705.
14. Liu, F.; Zhou, L.; Liu, W.; Zhou, Z.; Yue, Q.; Zheng, W.; Sun, R.; Liu, W.; Xu, S.; Fan, H.; et al. Organic Solar Cells with 18% Efficiency Enabled by an Alloy Acceptor: A Two–in–One Strategy. Adv. Mater. 2021, 33, 2100830.
15. Lin, Y.; Magomedov, A.; Firdaus, Y.; Kaltsas, D.; El–Labban, A.; Faber, H.; Naphade, D.R.; Yengel, E.; Zheng, X.; Yarali, E.; et al. 18.4 % Organic Solar Cells Using a High Ionization Energy Self–Assembled Monolayer as Hole–Extraction Interlayer. ChemSusChem 2021, 14, 3569–3578.
16. Li, Y.; Cai, Y.H.; Xie, Y.P.; Song, J.H.; Wu, H.B.; Tang, Z.; Zhang, J.; Huang, F.; Sun, Y.M. A facile strategy for third–component selection in non–fullerene acceptor–based ternary organic solar

cells. Energy Environ. Sci. 2021, 14, 5009–5016.

17. Cui, Y.; Xu, Y.; Yao, H.; Bi, P.; Hong, L.; Zhang, J.; Zu, Y.; Zhang, T.; Qin, J.; Ren, J.; et al. Single–Junction Organic Photovoltaic Cell with 19% Efficiency. Adv. Mater. 2021, 33, 2102420.
18. Chen, X.; Wang, D.; Wang, Z.; Li, Y.; Zhu, H.; Lu, X.; Chen, W.; Qiu, H.; Zhang, Q. 18.02% Efficiency ternary organic solar cells with a small–molecular donor third component. Chem. Eng. J. 2021, 424, 130397.
19. Cai, Y.; Li, Y.; Wang, R.; Wu, H.; Chen, Z.; Zhang, J.; Ma, Z.; Hao, X.; Zhao, Y.; Zhang, C.; et al. A Well–Mixed Phase Formed by Two Compatible Non–Fullerene Acceptors Enables Ternary Organic Solar Cells with Efficiency over 18.6%. Adv. Mater. 2021, 33, 2101733.
20. Mazzio, K.A.; Luscombe, C.K. The future of organic photovoltaics. Chem. Soc. Rev. 2015, 44, 78–90.
21. Hood, S.N.; Kassal, I. Entropy and Disorder Enable Charge Separation in Organic Solar Cells. J. Phys. Chem. Lett. 2016, 7, 4495–4500.
22. Scharber, M.C.; Sariciftci, N.S. Efficiency of bulk–heterojunction organic solar cells. Prog. Polym. Sci. 2013, 38, 1929–1940.
23. Gülen, D. Determination of the exciton diffusion length by surface quenching experiments. J. Lumin. 1988, 42, 191–195.
24. Hong, N.H.; Sakai, J.; Huong, N.T.; Poirot, N.; Ruyter, A. Role of defects in tuning ferromagnetism in diluted magnetic oxide thin films. Phys. Rev. B 2005, 72, 045336.
25. Zhang, R.; Yang, H.; Zhou, K.; Zhang, J.; Liu, J.; Yu, X.; Xing, R.; Han, Y. Optimized domain size and enlarged D/A interface by tuning intermolecular interaction in all–polymer ternary solar cells. J. Polym. Sci. Part B Polym. Phys. 2016, 54, 1811–1819.
26. Chen, S.; Zhang, L.; Ma, C.; Meng, D.; Zhang, J.; Zhang, G.; Li, Z.; Chow, P.C.Y.; Ma, W.; Wang, Z.; et al. Alkyl Chain Regiochemistry of Benzotriazole–Based Donor Polymers Influencing Morphology and Performances of Non–Fullerene Organic Solar Cells. Adv. Energy Mater. 2018, 8, 1702427.
27. Zhou, K.; Zhao, Q.; Zhang, R.; Cao, X.; Yu, X.; Liu, J.; Han, Y. Decreased domain size of p–DTS(FBTTh2)2/P(NDI2OD–T2) blend films due to their different solution aggregation behavior at different temperatures. Phys. Chem. Chem. Phys. 2017, 19, 32373–32380.
28. Xiao, B.; Du, M.; Wang, X.; Xiao, Z.; Li, G.; Tang, A.; Ding, L.; Geng, Y.; Sun, X.; Zhou, E. Effects of Oxygen Atoms Introduced at Different Positions of Non–Fullerene Acceptors in the Performance of Organic Solar Cells with Poly(3–hexylthiophene). ACS Appl. Mater. Interfaces 2020, 12, 1094–1102.

29. Zhou, K.; Wu, Y.; Liu, Y.F.; Zhou, X.B.; Zhang, L.; Ma, W. Molecular Orientation of Polymer Acceptor Dominates Open–Circuit Voltage Losses in All–Polymer Solar Cells. ACS Energy Lett. 2019, 4, 1057–1064.
30. Rand, B.P.; Cheyns, D.; Vasseur, K.; Giebink, N.C.; Mothy, S.; Yi, Y.; Coropceanu, V.; Beljonne, D.; Cornil, J.; Brédas, J.-L.; et al. The Impact of Molecular Orientation on the Photovoltaic Properties of a Phthalocyanine/Fullerene Heterojunction. Adv. Funct. Mater. 2012, 22, 2987–2995.
31. Zhang, Q.; Xiao, B.; Du, M.; Li, G.; Tang, A.; Zhou, E. A2–A1–D–A1–A2 type non–fullerene acceptors based on methoxy substituted benzotriazole with three different end–capped groups for P3HT–based organic solar cells. J. Mater. Chem. C 2018, 6, 10902–10909.
32. Xiao, B.; Tang, A.; Zhang, J.; Mahmood, A.; Wei, Z.; Zhou, E. Achievement of High Voc of 1.02 V for P3HT–Based Organic Solar Cell Using a Benzotriazole–Containing Non–Fullerene Acceptor. Adv. Energy Mater. 2017, 7, 1602269.
33. Qiu, N.L.; Yang, X.; Zhang, H.J.; Wan, X.J.; Li, C.X.; Liu, F.; Zhang, H.T.; Russell, T.P.; Chen, Y.S. Nonfullerene Small Molecular Acceptors with a Three–Dimensional (3D) Structure for Organic Solar Cells. Chem. Mater. 2016, 28, 6770–6778.
34. Liang, Q.; Han, J.; Song, C.; Yu, X.; Smilgies, D.-M.; Zhao, K.; Liu, J.; Han, Y. Reducing the confinement of PBDB–T to ITIC to improve the crystallinity of PBDB–T/ITIC blends. J. Mater. Chem. A 2018, 6, 15610–15620.
35. Liu, J.; Zeng, S.; Zhang, Z.; Peng, J.; Liang, Q. Optimizing the Phase–Separated Domain Size of the Active Layer via Sequential Crystallization in All–Polymer Solar Cells. J. Phys. Chem. Lett. 2020, 11, 2314–2321.
36. Xu, X.; Zhang, G.; Yu, L.; Li, R.; Peng, Q. P3HT–Based Polymer Solar Cells with 8.25% Efficiency Enabled by a Matched Molecular Acceptor and Smart Green–Solvent Processing Technology. Adv. Mater. 2019, 31, 1906045.
37. Yang, C.; Yu, R.; Liu, C.; Li, H.; Zhang, S.; Hou, J. Achieving over 10 % Efficiency in Poly(3–hexylthiophene)–based Organic Solar Cells via Solid Additives. ChemSusChem 2021, 14, 3607–3613.
38. Liu, F.; Zhang, J.Y.; Zhou, Z.C.; Zhang, J.Q.; Wei, Z.X.; Zhu, X.Z. Poly(3–hexylthiophene)–based non–fullerene solar cells achieve high photovoltaic performance with small energy loss. J. Mater. Chem. A 2017, 5, 16573–16579.
39. Li, S.; Liu, W.; Shi, M.; Mai, J.; Lau, T. –K.; Wan, J.; Lu, X.; Li, C.–Z.; Chen, H. A spirobifluorene and diketopyrrolopyrrole moieties based non–fullerene acceptor for efficient and thermally stable polymer solar cells with high open–circuit voltage. Energy Environ. Sci. 2016, 9, 604–610.

40. Holliday, S.; Ashraf, R.S.; Wadsworth, A.; Baran, D.; Yousaf, S.A.; Nielsen, C.B.; Tan, C.H.; Dimitrov, S.D.; Shang, Z.; Gasparini, N.; et al. High–efficiency and air–stable P3HT–based polymer solar cells with a new non–fullerene acceptor. Nat. Commun. 2016, 7, 11585.
41. Liu, J.G.; Zeng, S.Y.; Jing, P.; Zhao, K.; Liang, Q.J. Investigating the effect of cosolvents on P3HT/O–IDTBR film–forming kinetics and film morphology. J. Energy. Chem. 2020, 51, 333–341.
42. Liang, Q.; Jiao, X.; Yan, Y.; Xie, Z.; Lu, G.; Liu, J.; Han, Y. Separating Crystallization Process of P3HT and O–IDTBR to Construct Highly Crystalline Interpenetrating Network with Optimized Vertical Phase Separation. Adv. Funct. Mater. 2019, 29, 1807591.
43. Gaspar, H.; Figueira, F.; Pereira, L.; Mendes, A.; Viana, J.C.; Bernardo, G. Recent Developments in the Optimization of the Bulk Heterojunction Morphology of Polymer: Fullerene Solar Cells. Materials 2018, 11, 2560.
44. Wang, X.; Sun, Q.; Gao, J.; Wang, J.; Xu, C.; Ma, X.; Zhang, F. Recent Progress of Organic Photovoltaics with Efficiency over 17%. Energies 2021, 14, 4200.
45. Liao, K.-S.; Yambem, S.D.; Haldar, A.; Alley, N.J.; Curran, S.A. Designs and Architectures for the Next Generation of Organic Solar Cells. Energies 2010, 3, 1212–1250.
46. Zhao, Y.; Yuan, G.X.; Roche, P.; Leclerc, M. A Calorimetric Study of the Phase–Transitions in Poly(3–Hexylthiophene). Polymer 1995, 36, 2211–2214.
47. Dittmer, J.J.; Lazzaroni, R.; Leclere, P.; Moretti, P.; Granstrom, M.; Petritsch, K.; Marseglia, E.A.; Friend, R.H.; Bredas, J.L.; Rost, H.; et al. Crystal network formation in organic solar cells. Sol. Energy Mater Sol. Cells 2000, 61, 53–61.
48. Padinger, F.; Rittberger, R.S.; Sariciftci, N.S. Effects of postproduction treatment on plastic solar cells. Adv. Funct. Mater. 2003, 13, 85–88.
49. Jenekhe, S.A.; Yi, S.J. Highly photoconductive nanocomposites of metallophthalocyanines and conjugated polymers. Adv. Mater. 2000, 12, 1274.
50. Ma, W.; Yang, C.; Gong, X.; Lee, K.; Heeger, A.J. Thermally Stable, Efficient Polymer Solar Cells with Nanoscale Control of the Interpenetrating Network Morphology. Adv. Funct. Mater. 2005, 15, 1617–1622.
51. Lee, H.; Oh, S.; Song, C.E.; Lee, H.K.; Lee, S.K.; Shin, W.S.; So, W.W.; Moon, S.J.; Lee, J.C. Stable P3HT: Amorphous non–fullerene solar cells with a high open–circuit voltage of 1 V and efficiency of 4%. RSC Adv. 2019, 9, 20733–20741.
52. Jang, M.; Huh, Y.I.; Chang, M. Effects of Solvent Vapor Annealing on Morphology and Charge Transport of Poly(3–hexylthiophene) (P3HT) Films Incorporated with Preformed P3HT Nanowires. Polymers 2020, 12, 1188.

53. Li, G.; Shrotriya, V.; Huang, J.; Yao, Y.; Moriarty, T.; Emery, K.; Yang, Y. High–efficiency solution processable polymer photovoltaic cells by self–organization of polymer blends. Nat. Mater. 2005, 4, 864–868.
54. Wu, J.; Yuan, Y.; Gao, M.; Wang, Z.; Jiang, L. Preparation of Single Crystals of Small Molecule Organic Semiconductor via Solvent Vapor Annealing. Acta Chim. Sin. 2015, 73, 23–28.
55. Vogelsang, J.; Brazard, J.; Adachi, T.; Bolinger, J.C.; Barbara, P.F. Watching the Annealing Process One Polymer Chain at a Time. Angew. Chem. Int. Ed. 2011, 50, 2257–2261.
56. Hammed, W.; Yahya, R.; Bola, A.u.; Mahmud, H. Recent Approaches to Controlling the Nanoscale Morphology of Polymer–Based Bulk–Heterojunction Solar Cells. Energies 2013, 6, 5847–5868.
57. Yang, L.; Zhang, S.; He, C.; Zhang, J.; Yao, H.; Yang, Y.; Zhang, Y.; Zhao, W.; Hou, J. New Wide Band Gap Donor for Efficient Fullerene–Free All–Small–Molecule Organic Solar Cells. J. Am. Chem. Soc. 2017, 139, 1958–1966.
58. Chang, Y.M.; Wang, L. Efficient Poly(3–hexylthiophene)–Based Bulk Heterojunction Solar Cells Fabricated by an Annealing–Free Approach. J. Phys. Chem. C 2008, 112, 17716–17720.
59. Berson, S.; De Bettignies, R.; Bailly, S.; Guillerez, S. Poly(3–hexylthiophene) Fibers for Photovoltaic Applications. Adv. Funct. Mater. 2007, 17, 1377–1384.
60. Yang, D.; Yu, K.; Xu, J.; Zhang, J.; Zhang, J.; Gao, J.; Song, W.; Li, D.; Chen, Z.; Ge, Z. Achieving 10% efficiency in non–fullerene all–small–molecule organic solar cells without extra treatments. J. Mater. Chem. A 2021, 9, 10427–10436.
61. Wan, J.; Wen, R.; Xia, Y.; Dai, M.; Huang, H.; Xue, L.; Zhang, Z.; Fang, J.; Hui, K.N.; Fan, X. All annealing–free solution–processed highly flexible organic solar cells. J. Mater. Chem. A 2021, 9, 5425–5433.
62. Kazerouni, N.; Melenbrink, E.L.; Das, P.; Thompson, B.C. Ternary Blend Organic Solar Cells Incorporating Ductile Conjugated Polymers with Conjugation Break Spacers. ACS Appl. Polym. Mater. 2021, 3, 3028–3037.
63. Avalos–Quiroz, Y.A.; Bardagot, O.; Kervella, Y.; Aumaitre, C.; Cabau, L.; Rivaton, A.; Margeat, O.; Videlot–Ackermann, C.; Vongsaysy, U.; Ackermann, J.; et al. Non–Fullerene Acceptors with an Extended pi–Conjugated Core: Third Components in Ternary Blends for High–Efficiency, Post–Treatment–Free Organic Solar Cells. ChemSusChem 2021, 14, 3502–3510.
64. Buss, F.; Schmidt–Hansberg, B.; Sanyal, M.; Munuera, C.; Scharfer, P.; Schabel, W.; Barrena, E. Gaining Further Insight into the Solvent Additive–Driven Crystallization of Bulk–Heterojunction Solar Cells by in Situ X–ray Scattering and Optical Reflectometry. Macromolecules 2016, 49, 4867–4874.

65. Park, S.H.; Jin, I.S.; Ahn, H.; Jung, J.W. Non–halogenated additive engineering for morphology optimization in environmental–friendly solvent processed non–fullerene organic solar cells. Org. Electron. 2020, 86, 105893.
66. Kırbıyık Kurukavak, Ç.; Yılmaz, T.; Çetin, Ş.; Alqadasi, M.M.; Al–Khawlany, K.M.; Kuş, M. Synthesis of boron–doped CQDs and its use as an additive in P3HT:PCBM layer for efficiency improvement of organic solar cell. Microelectron. Eng. 2021, 235, 111465.
67. Arbab, E.A.A.; Gebremichael, B.; Kumar, A.; Mola, G.T. Morphology–dependent performance of thin film organic solar cells. J. Mod. Opt. 2018, 66, 399–406.
68. Alam, S.; Islam, M.M.; Chowdhury, S.; Meitzner, R.; Kästner, C.; Schubert, U.S.; Hoppe, H. Disentanglement of Degradation Mechanisms by Analyzing Aging Dynamics of Environmentally Friendly Processed Polymer Solar Cells. Energy Technol. 2020, 8, 2000116.
69. Shin, N.; Richter, L.J.; Herzing, A.A.; Kline, R.J.; DeLongchamp, D.M. Effect of Processing Additives on the Solidification of Blade–Coated Polymer/Fullerene Blend Films via In–Situ Structure Measurements. Adv. Energy Mater. 2013, 3, 938–948.
70. Zhu, L.; Zhong, W.; Qiu, C.; Lyu, B.; Zhou, Z.; Zhang, M.; Song, J.; Xu, J.; Wang, J.; Ali, J.; et al. Aggregation–Induced Multilength Scaled Morphology Enabling 11.76% Efficiency in All–Polymer Solar Cells Using Printing Fabrication. Adv. Mater. 2019, 31, 1902899.
71. Li, W.; Chen, M.; Zhang, Z.; Cai, J.; Zhang, H.; Gurney, R.S.; Liu, D.; Yu, J.; Tang, W.; Wang, T. Retarding the Crystallization of a Nonfullerene Electron Acceptor for High–Performance Polymer Solar Cells. Adv. Funct. Mater. 2018, 29, 1807662.
72. Zhou, K.; Zhang, R.; Liu, J.; Li, M.; Yu, X.; Xing, R.; Han, Y. Donor/Acceptor Molecular Orientation–Dependent Photovoltaic Performance in All–Polymer Solar Cells. ACS Appl. Mater. Interfaces 2015, 7, 25352–25361.
73. Li, M.; Zhou, Y.; Yang, L.; Shen, S.; Liu, Y.; Chen, Y.; Song, J.; Bo, Z. Regulating molecular orientations of dipyran–based nonfullerene acceptors through side–chain engineering at the π–bridge. J. Mater. Chem. A 2020, 8, 22416–22422.
74. Lee, C.; Li, Y.; Lee, W.; Lee, Y.; Choi, J.; Kim, T.; Wang, C.; Gomez, E.D.; Woo, H.Y.; Kim, B.J. Correlation between Phase–Separated Domain Sizes of Active Layer and Photovoltaic Performances in All–Polymer Solar Cells. Macromolecules 2016, 49, 5051–5058.
75. Chen, J.; Bi, Z.; Xu, X.; Zhang, Q.; Yang, S.; Guo, S.; Yan, H.; You, W.; Ma, W. Fine Optimization of Morphology Evolution Kinetics with Binary Additives for Efficient Non–Fullerene Organic Solar Cells. Adv. Sci. 2019, 6, 1801560.
76. Lee, J.K.; Ma, W.L.; Brabec, C.J.; Yuen, J.; Moon, J.S.; Kim, J.Y.; Lee, K.; Bazan, G.C.; Heeger, A.J. Processing Additives for Improved Efficiency from Bulk Heterojunction Solar Cells. J. Am. Chem. Soc. 2008, 130, 3619–3623.

77. Sun, Y.; Liu, J.-G.; Ding, Y.; Han, Y.-C. Controlling the surface composition of PCBM in P3HT/PCBM blend films by using mixed solvents with different evaporation rates. Chin. J. Polym. Sci. 2013, 31, 1029–1037.

Retrieved from https://encyclopedia.pub/entry/history/show/38648